ADVANCED FUNCTIONAL MATERIALS
www.afm-journal.de

Screening Mesenchymal Stem Cell Attachment and Differentiation on Porous Silicon Gradients

Peng-Yuan Wang, Lauren R. Clements, Helmut Thissen, Andrew Jane, Wei-Bor Tsai, and Nicolas H. Voelcker**

The profound effects that nanoscale surface topography exerts on cell behavior are highly relevant to the development of advanced biomaterials and to advances in tissue engineering and regenerative medicine. Here, an asymmetric anodization procedure is used to produce n-type porous silicon (pSi) gradients with pore sizes ranging from tens to hundreds of nanometers in diameter and changes in the ridge nanoroughness from a few to tens nanometers. Rat mesenchymal stem cells (rMSCs) adhere poorly at the regions with small pore size but high ridge roughness. Cell adhesion is increased gradually towards the large pore size but low ridge roughness end of the pSi gradients. Surface topography influences cell differentiation, but not cell proliferation. Osteogenesis of rMSCs is enhanced by porous topography with a ridge roughness lower than 10 nm, while adipogenesis of rMSCs is enhanced on the entire pSi gradient compared with flat Si substrates. The results demonstrate that the gradient format allows in-depth screening of surface parameters that are important for the control of mammalian cell behavior, thereby advancing the development of new and improved biomaterials for orthopaedic and tissue engineering applications.

1. Introduction

The ability to direct cell behavior by means of biomaterial surface topography is of critical importance for biomedical and tissue engineering applications.[1] Substrate topography has been shown to be an effective cue for the regulation of cellular responses, including stem cell responses.[2,3] Cell attachment, migration, proliferation and differentiation can be effectively regulated by various topographic features such as pores[4] and grooves[5,6] with dimensions ranging from the nano- to the microscale.[7] Because cellular responses to these surface topographies are feature size-dependent, surface topographies with various feature sizes have been fabricated separately. However, analysis and screening of discrete, individual samples is a tantalizing task due to the large combinatorial space to be analyzed. Therefore, a surface topography gradient-based approach is desirable since it enables the screening of cellular responses in high throughput, significantly reducing the time required for sample preparation and analysis and allowing the fine-tuning of surface characteristics in a single experiment.

Porous silicon (pSi) is fabricated by electrochemical anodic etching of silicon wafers in electrolytes containing hydrofluoric acid (HF).[8] Cellular responses to and the biocompatibility of this nanostructured material have been investigated in vitro and in vivo.[8–11] The porosity, pore size and pore structure of pSi can be tuned by varying the etching conditions to generate surfaces with high surface area (>600 $m^2 g^{-1}$) and pore size ranging from a few nanometers to several micrometers.[12] Furthermore, the surface chemistry of pSi can be controlled by oxidation and silanization[13] or, alternatively, by reactions involving the hydride-terminated freshly etched surface, the most popular of those being hydrosilylation.[14,15] Recently, the fabrication of pSi displaying a pore size gradient has been demonstrated on a p-type silicon wafer.[16–18] By controlling several parameters such as current density, HF-to-surfactant ratio and the doping/resistivity of wafers, the pore size distribution of pSi can be easily controlled along a silicon surface.[17] Using these pSi gradients, the adhesion of human neuroblastoma cells was found to be highly sensitive to pore size, resulting in cells adhering well on the gradient end displaying large pores (1-3 μm), forming long and thick neurite processes, but adhering poorly on the middle of the gradient (100-300 nm pores). A gradual recovery of the typical neuroblastoma cell morphology occurred for neuroblastoma cells growing on mesoporous (<50 nm pores) pSi. This study highlighted the potential of investigating cellular responses using a pore size gradient format.

Dr. P.-Y. Wang, Prof. W.-B- Tsai
Department of Chemical Engineering
National Taiwan University
No. 1, Roosevelt Rd., Sec. 4, Taipei, 106, Taiwan
E-mail: weibortsai@ntu.edu.tw
Dr. P.-Y. Wang, L. R. Clements, A. Jane
School of Chemical and Physical Sciences
Flinders University
Bedford Park, SA 5042, Australia
Dr. H. Thissen
CSIRO Materials Science and Engineering
Bayview Avenue, Clayton VIC 3168, Australia
Prof. N. H. Voelcker
Mawson Institute
University of South Australia
Mawson Lakes, SA 5095, Australia
E-mail: nico.voelcker@unisa.edu.au

DOI: 10.1002/adfm.201200447

Despite the potential advantages of pSi gradients as a screening tool for studying cell-surface interactions, studies using this format are still rare. This is due to the instability of the pSi layer under cell culture conditions.[19,20] Whilst smooth crystalline silicon degrades extremely slowly,[21] pSi degrades in an aqueous environment into silicic acid.[22] Moreover, although various surface chemistries have been applied to increase the stability of pSi,[19,23] the issue of pore degradation and collapse during prolonged cell culture has not been resolved.[20] This instability of the pSi layer prevents it from applications requiring long-term cell culture such as stem cell differentiation that usually requires several weeks of culture.[14,20] For example, in order to explore the fate of mesenchymal stem cells (MSCs), an important cell source for regenerative medicine due to its differentiation potential into several cell lineages such as bone, cartilage and muscle,[24] by presenting a gradient of surface topography would require more stable pSi gradient substrates.[25]

The purpose of the present study was to develop stable pSi gradients for long-term culture and to investigate the dependence of the differentiation of MSCs on surface porous topography. We found that n-type pSi gradients after surface oxidation and subsequent amino-silanization were sufficiently stable to investigate the differentiation of MSCs into bone- or fat-like cells over a period of four weeks.

2. Results and Discussion

2.1. Fabrication and Pore Size Distribution of n-pSi Gradients

The setup of the porous silicon (pSi) gradient fabrication was the same as described in a previous study,[17] positioning the electrode vertically to the silicon surface at one end of a custom-built PTFE etching cell (Supporting Information, Figure s1). However, pore size gradients could not be fabricated along the surface by applying a low etching current density (40-60 mA cm^{-2}) for a period of time (50 s) (Supporting Information, Figure s2). For highly doped n-type silicon wafers, illumination is not required to porosify the material.[26] We used a current density of 300 mA cm^{-2} for 1.7 s to create a pore size gradient on n-type Si. Observed using atomic force microscopy (AFM), a topography gradient was generated along the surface of n-type Si from 0 mm to 12 mm (Supporting Information, Figure s3). Under these conditions pores were small underneath the electrode (0 mm), and the pore sizes were gradually increased away from the electrode. The porous layer was extremely shallow due to the short etching period. To fabricate a thicker pSi layer, another etching was applied subsequently with a current density of 45 mA cm^{-2} for 50 s, resulting in a successive two-step etching procedure for n-type pSi (n-pSi) gradient fabrication. High voltage during the first etching resulted in electropolishing and the corresponding silver color at the location of the electrode (**Figure 1**). As observed from AFM and scanning electron microscopy (SEM), this two-step etching procedure generated a thicker porous layer of pSi and a pore size gradient along the surface from 0 mm to 12 mm of the gradients (**Figure 2**). Moreover, the small pores were found underneath

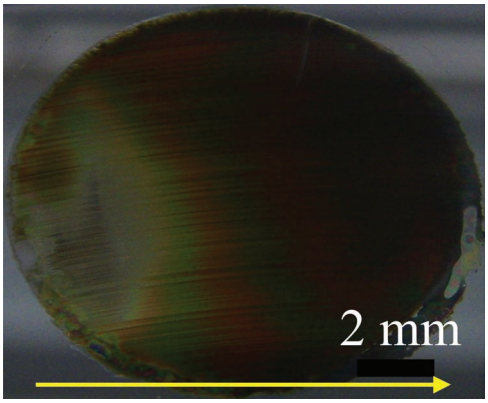

Figure 1. Photograph of asymmetrically anodised porous silicon surface etched on n-type silicon. The arrow shows the direction of the electrical field. The area below the electrode was electropolished and appeared silver (left-hand side of sample). Different colors (right-hand side of sample) along the gradient are due to reflective interference effects.

the large pores at the 12 mm of the gradients (Figure 2A,c). This finding suggests that two layers were formed during the two-step etchings. Although this two-step etching procedure generated two layers, the boundary between the two layers was difficult to distinguish as the first layer was very thin due to the very short etching period and the second layer might not affect cell behavior directly. The above result confirmed our hypothesis that a thicker n-pSi gradient can be fabricated based on a two-step etching procedure.

On the n-pSi gradients, a combination of large pores and small pores appeared on the surface (Figure 2 and **Figure 3**). The small pores (~30 nm diameter) appeared over the entire length of the gradient (0-12 mm), whilst the large pores appeared from approximately 6 mm of the gradients (~140 nm diameter), increasing in frequency and sizes to the 12 mm of the gradients (~310 nm diameter) (Figure 3A). At the location underneath the electrode (0 mm), the average pore diameter was 29 ± 12 nm. Both the large pores appearing and their frequency increasing contributed to an increase in average pore size from the 6 mm to the 12 mm of the gradient. At the distal end of the gradient (12 mm), the number ratio and area ratio of large pores was ~70% and ~93%, respectively (Figure 3B and 3C), resulting in an average pore size of 226 ± 37 nm. Interestingly, the pore size distribution of the n-pSi gradient was followed an opposite trend to the distribution observed for p-type pSi gradients, where the largest pores were observed at the location underneath the electrode (0 mm).[16,17] The difference between n-type and p-type pSi gradient is due to the different etching procedure. When using a two-step etching procedure on p-type Si, an increase in the average pore size from the location underneath the electrode (0 mm) to the distal end of the gradient (12 mm) was also observed (Supporting Information, Figure 4). The porous layer of the n-pSi gradient was about 800 nm in thickness at the position 0 mm, and about 1.2 μm in thickness for the remainder of the gradient (from 4 mm to 12 mm of the gradient) (Figure 3D). Electropolishing at the position of the electrode resulted in a reduced porous layer thickness.

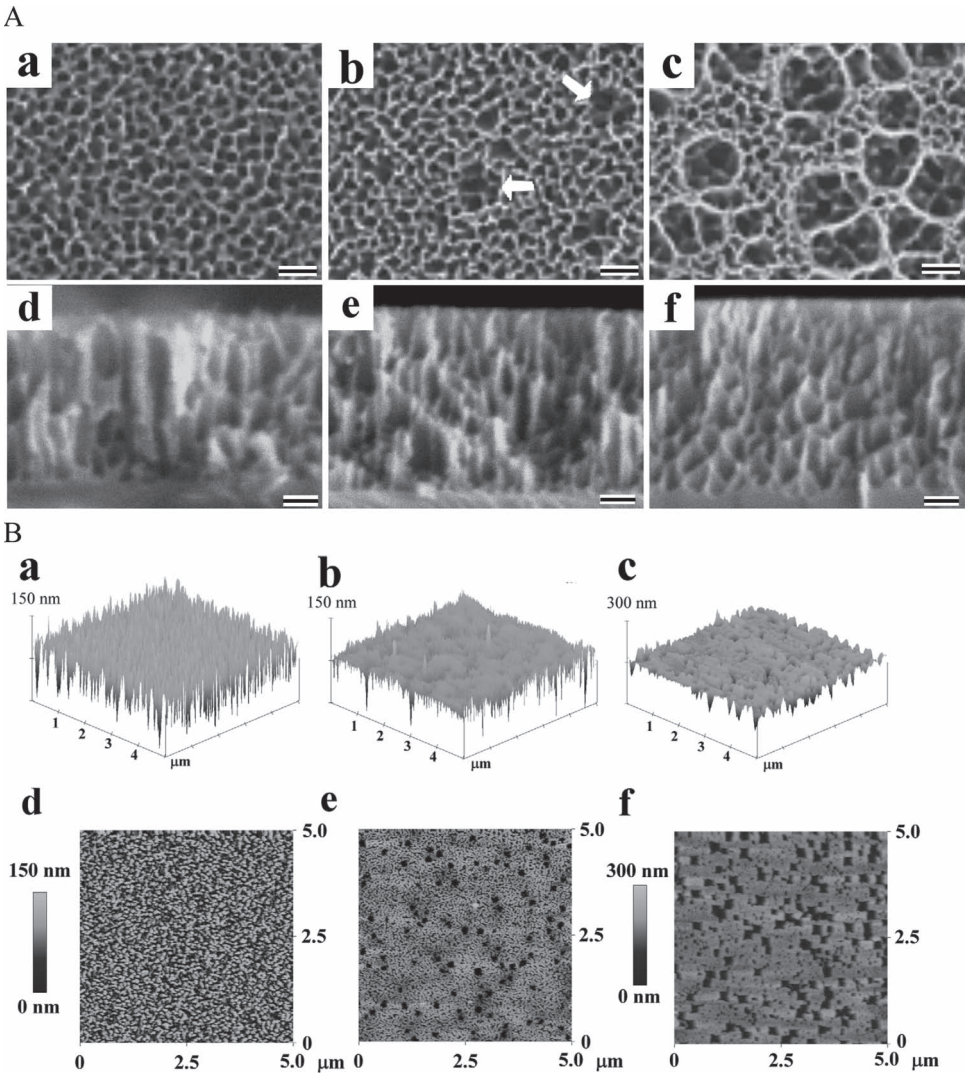

Figure 2. A) Scanning electron microscopy (SEM) images of n-type pSi gradients showing a–c) top view and d–f) cross-section view. Arrows in image (b) indicate the appearance of large pores. Scale bar = 200 nm. B) Atomic force microscopy (AFM) images of n-type pSi gradients a–c) 45° view and d–f) top view. Three positions representing the location underneath the electrode (0 mm), the middle of the gradient (6 mm), and the distal end of the gradient (12 mm) are shown from left to right, respectively.

2.3. Solid Surface Fraction and Ridge Roughness of n-pSi Gradients

Ridge roughness and solid surface fraction (solid area/total surface area) along the n-pSi gradients were analyzed by AFM and SEM, respectively. The solid surface fraction of the n-pSi gradient showed a slight decrease of about 20% from the 0 mm (56 ± 8%) to the 12 mm position of the gradients (37 ± 8%, **Figure 4**A). The ridge roughness of the n-pSi gradient was also found to decrease from the 0 mm (Ra = 22.29 ± 1.21 nm) to the 12 mm position of the gradients (Ra = 3.15 ± 0.02 nm, Figure 4B). In comparison, the surface roughness of flat Si was Ra = 0.49 ± 0.01 nm. From the microscopy images and analysis, the topography of n-pSi gradient at the location underneath the electrode (0 mm) was gradually changed along the direction of electrical field and was far different from the topography at the distal end of gradient (12 mm).

2.4. Surface Stabilization and Hydrophilicity

To stabilize the porous layer and increase cell affinity, the n-pSi gradients were treated by thermal oxidation followed by ozone oxidation to introduce silanol groups, and finally by coating with 3-aminopropyltriethoxysilane (APTES). The oxidation process increases the stability and biocompatibility of pSi[13] and amino-functionalization further enhances MSC adhesion.[27] Infrared spectroscopy showed that amino groups were introduced on the n-type Si surface, indicating that the APTES conjugation was successful (Supporting Information, Figure s5). Water contact angle (WCA) measurements showed that the n-pSi gradients were superhydrophobic before modification (WCA ~ 150°) (**Table 1**). Here, the WCA along the entire n-pSi gradient was approximately 150°. After the sequence of surface modifications carried out in this study, the wettability of n-pSi was increased significantly. The WCA measured along

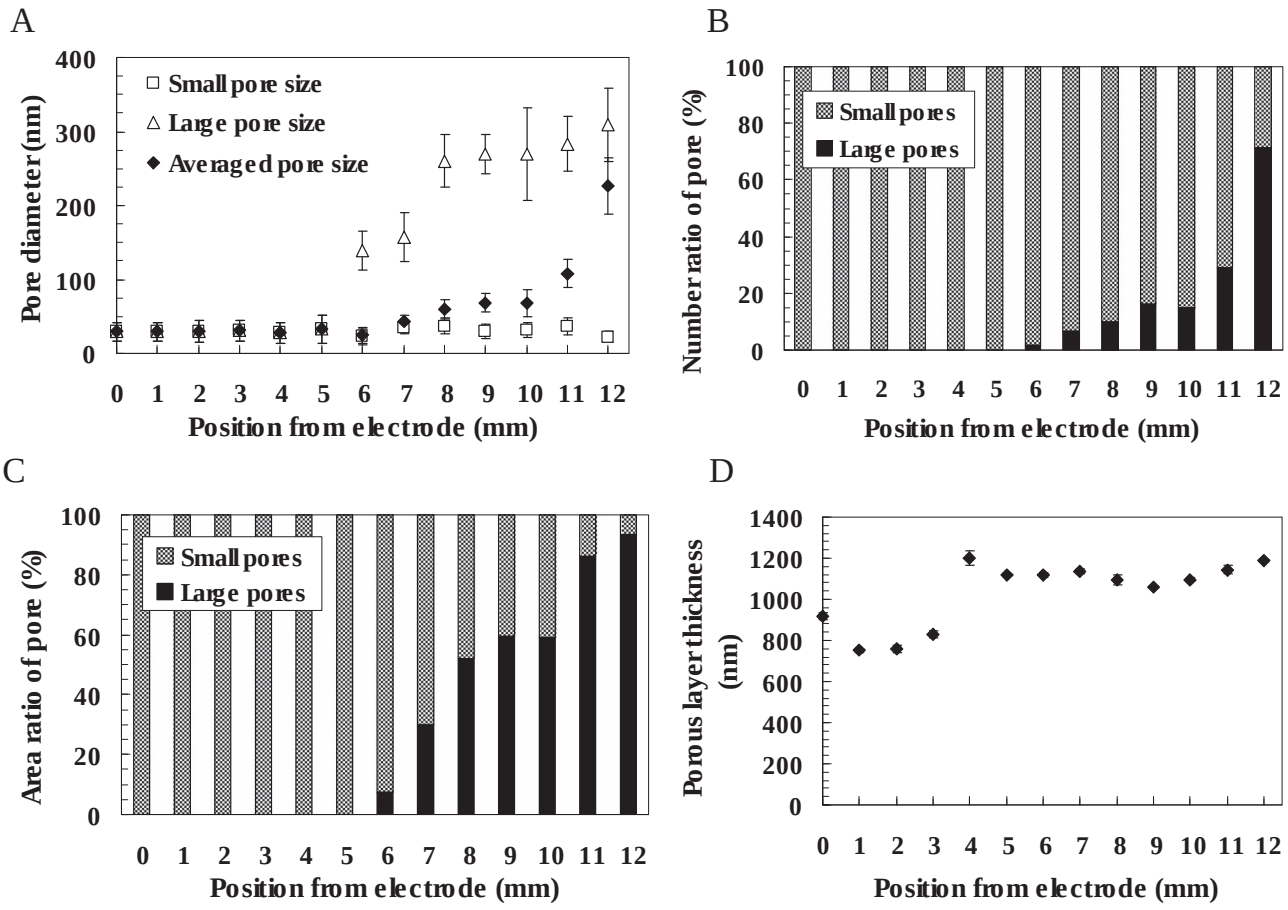

Figure 3. A) Average pore diameter, B) number ratio of pore, C) area ratio of pore size, and D) porous layer thickness of n-type pSi gradients. Number of analyzed pores > 200. Error bar = standard deviation. Error bars are not seen at some data points due to a low error.

the entire n-pSi gradient was approximately 12°, while the WCA measured on the flat Si was approximately 73°.

The above results indicate that both the surface topography and chemistry modulate the surface wettability (porous vs. flat or before vs. after surface modification). Wenzel and Cassie models[28,29] explain that low surface energy with high surface roughness results in a high value of WCA (often referred to as the Lotus Effect). However, if the surface has a high surface energy, surface roughness facilitates the decrease of WCA. On fresh pSi, the surface energy is low. Porous structure enhances the hydrophobicity of the surface. After surface modifications (APTES-coated pSi), surface energy of the n-pSi gradients is increased. The large surface area of pSi facilitates the wetting, resulting in a dramatically decrease in WCA. The similar phenomena has been found for submicron grooved topographies.[30]

2.5. rMSCs Attachment on n-pSi Gradients

Rat mesenchymal stem cells (rMSCs) were cultured for 24 h on the n-pSi gradients to determine the effect of the topography on cell attachment and morphology. Judging from the fluorescence microscopy and SEM images, cell attachment on the n-pSi gradient, with respect to the number and spreading of adhered cells, and the formation of actin filaments, was poor at the location 0 mm of the gradients, with cells showing round morphology (**Figure 5**a,g). Cells attached well and fully spread out at 12 mm of the gradients and on flat Si (Figure 5f,l). Cell density was the lowest at 0 mm ($0.35 \pm 0.05 \times 10^4$ cell cm^{-2}), gradually increased to 6 mm ($0.60 \pm 0.04 \times 10^4$ cell cm^{-2}), and reached a peak value at 12 mm of the gradients ($1.28 \pm 0.02 \times 10^4$ cell cm^{-2}) (Figure 5a–e and 5g–k). Cell density was $1.66 \pm 0.08 \times 10^4$ cell cm^{-2} on the flat Si.

A previous study has suggested that pore size of pSi gradient affected human neuroblastoma cell adhesion,[17] Likewise, surface roughness of titanium has been shown to modulate human osteoblastic cell adhesion.[31] Among the surface properties along the n-pSi gradients, we propose that focal adhesion formation is the key factor to direct rMSC adhesion on the surface. Both pore size and surface roughness determines the focal adhesion formation.[32] When the pore size and surface roughness increase, cell-substrate contact would decrease. Therefore, cell adhesion would have a reverse trend regarding the pore size and roughness distributions. On the n-type pSi gradient, the average pore size was similar from 0 mm to 5 mm (~30 nm) and increased from 6 mm (138 ± 26 nm) to 12 mm (226 ± 37 nm) of the gradient. Cell adhesion is not satisfied the above

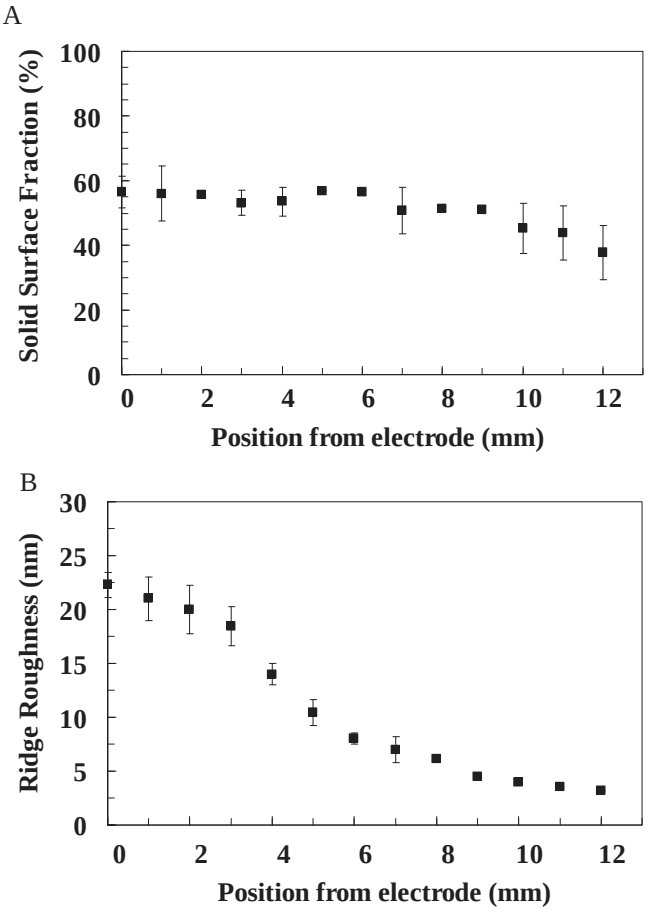

Figure 4. A) Solid surface fraction and B) ridge roughness of n-type pSi gradients. Solid surface fraction = solid area/total area in the image (n = 6). Ridge roughness = roughness of a selected area of AFM images on the ridge (n = 6). Error bar = standard deviation. Error bars are not seen at some data points due to a low error.

hypothesis that cell density should decrease from 0 mm to 12 mm of the gradient. On the contrary, cell density increased gradually from 0 mm to 12 mm of the gradient, while the ridge roughness decreased gradually from 0 mm (Ra = 22.29 ± 1.21 nm) to 12 mm (Ra = 3.15 ± 0.02 nm) of the gradient, suggesting that the ridge roughness dominated the rMSC adhesion on the n-type pSi gradients. One previous study reported that MC3T3-E1 osteoblastic cells adhered poorly on a surface topography with high surface roughness that the structure is similar to the presenting location 0 mm,[33] suggesting that high roughness appears to inhibit rMSCs adhesion at the location underneath the electrode, resulting in a cell density gradient and ridge roughness gradient with an inverse correlation along the n-pSi surface.

Table 1. Water contact angle (WCA) of n-type pSi gradients. WCA at five different positions along the surface from the electrode site to the distal end of the gradient as well as at flat Si were analyzed before (fresh) and after surface modifications (amino-silanization).

Position from Pt electrode	Fresh pSi	Modified pSi
0 mm	145.0 ± 7.5	12.6 ± 2.2
3 mm	154.1 ± 2.7	10.5 ± 2.7
6 mm	152.7 ± 2.4	12.9 ± 3.3
9 mm	152.7 ± 0.9	12.0 ± 3.1
12 mm	147.9 ± 5.0	11.2 ± 5.5
Flat	46.6 ± 6.5***	73.1 ± 6.3***

***, $p < 0.001$ compared with the porous area (n = 6).

2.6. rMSCs Proliferation on n-pSi Gradients

At the location 0 mm of the n-pSi gradient, the area with the lowest cell affinity, the cell density increased from 0.65 ± 0.19 × 10^4 cells cm^{-2} at day 1 to 1.66 ± 0.28 × 10^4 cell cm^{-2} at day 6, but did not reach confluence (**Figure 6**A). As those rMSCs attached to this region of the gradient initially displayed a round morphology, they tended to form cell clusters after a 6 day culture period (Figure 6B,a and e). These observations suggest that the surface topography at 0 mm is unfavorable to rMSCs adhesion and spreading, and that cell-cell contacts are preferred over cell-surface interactions. On the other hand, cell density gradually increased from 0 mm to 12 mm of the gradient, and it increased from 1.36 ± 0.54 × 10^4 cells cm^{-2} at day 1 to 2.95 ± 0.49 × 10^4 cells cm^{-2} at day 6 with confluence at location 12 mm, and significant higher than that at the location 0 mm ($p < 0.001$). In this region (location 12 mm), rMSCs formed stable contacts with the surface and exhibited spread morphology. Both cell density and morphology at 12 mm of the gradient were comparable with that on the flat Si, where the density increased from 2.06 ± 0.30 × 10^4 cells cm^{-2} at day 1 to 3.35 ± 0.98 × 10^4 cells cm^{-2} at day 6.

Cell proliferation is a subsequent event after cell adhesion and an important event preceding cell differentiation.[34] It is known that cell proliferation can be modulated by cell-surface interactions and local cell density.[35] Surface topography at the 0 mm of the gradient suppressed cell adhesion and spreading, but did not retard the proliferation of rMSCs. It is possible that low local cell density allows cells to proliferate. Cells tend to aggregate to each other, stabilize themselves on the surface via cell-cell contacts,[36] and, subsequently, proliferate through cell-cell contacts.[27] On the other hand, cell morphology was gradually spread out toward the end of the gradient and fully spread out with a high cell density at 12 mm of the gradient as well as on the flat Si, revealing more favourable surface properties in these regions. Although the proliferation rate at each position along the gradient was similar (~2.1-2.5 fold), the morphology and density was different from the 0 mm to 12 mm of the gradient. In other words, after 6 day culture, there was still a cell morphology and density gradient observed along the n-pSi gradient.

2.7. Osteogenesis and Adipogenesis of rMSCs on n-pSi Gradients

After 3-week osteogenic induction, rMSCs gradually became bone-like cells and formed bone nodule-like colonies (**Figure 7**). Calcium deposits were stained with Calcein Blue (CB), indicating the extent of the mineralization in osteogenic

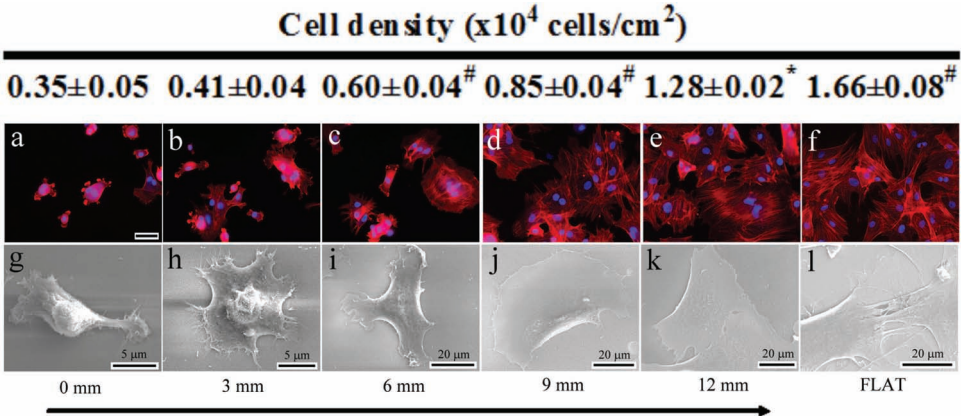

Figure 5. a–f) Cytoskeleton staining and g–l) SEM images of rat mesenchymal stem cells (rMSCs) on n-type pSi gradients after 24 h culture. The merged images of nuclei and F-actin staining and SEM images were displayed from 0 mm (location underneath the electrode) to 12 mm of the gradients. FLAT = flat Si. The arrow underneath the figure shows the direction of the electrical field. Scale bar = 50 μm in fluorescent images. Cell density of rMSCs on n-type pSi gradients was quantified at each position after 24 h culture. Value = mean ± standard deviation ($n = 3$). The number of counted nuclei was 278-365. # and * represent $p < 0.01$ and $p < 0.001$, respectively, compared with the previous position from the electrode.

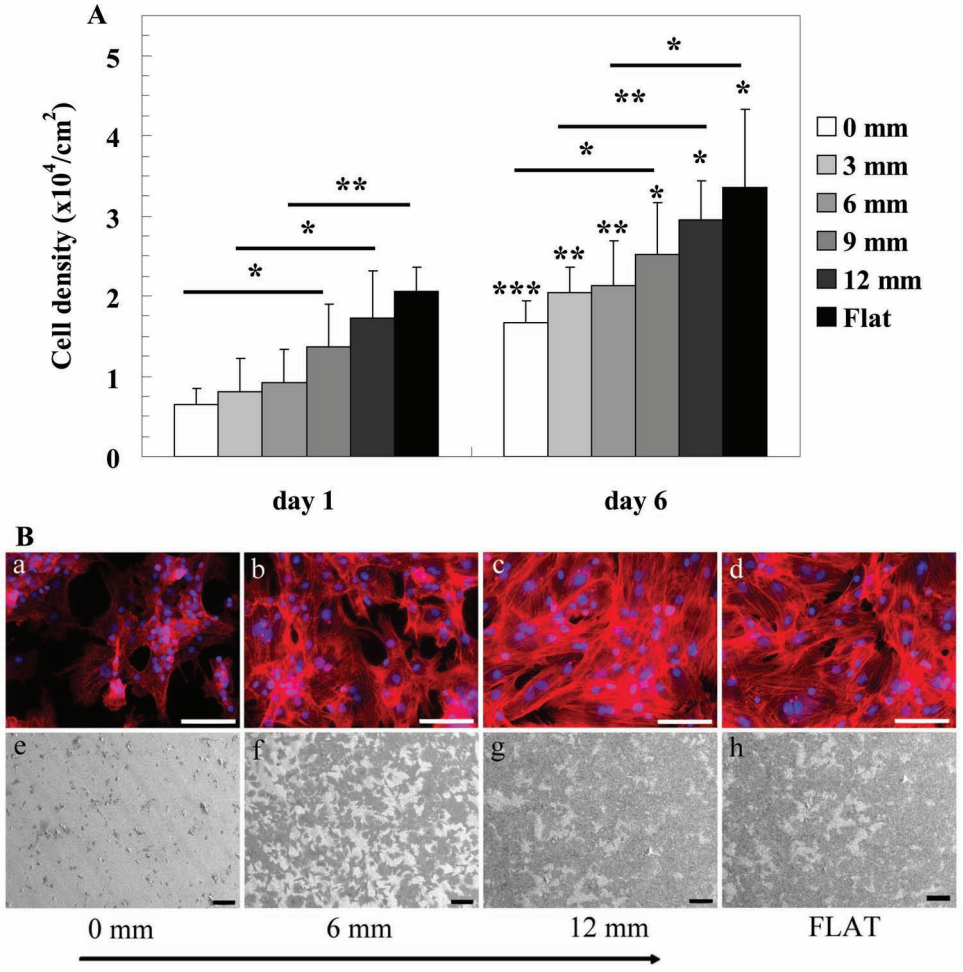

Figure 6. A) Cell proliferation from day 1 to day 6 and B) cell morphology on n-type pSi gradients after 6 days of culture. The number of counted nuclei was 105-556. *, **, and *** represent $p < 0.05$, $p < 0.01$ and $p < 0.001$, respectively ($n = 5$). Error bar = standard deviation. The merged images of nucleus and F-actin staining and SEM images are displayed from 0 mm (location underneath the electrode) to 12 mm of the gradients. FLAT = flat Si. The arrow underneath the figure shows the direction of the electrical field. Scale bar = 100 μm in fluorescent images and 200 μm in SEM images.

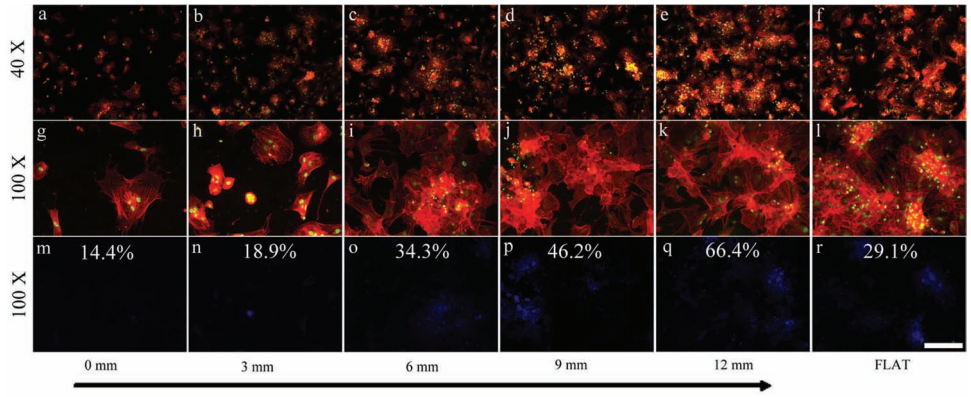

Figure 7. Osteogenesis of rMSCs on the n-type pSi gradients after 3 week induction with a–l) representing merged images of nuclei (PICO Green) and F-actin (TRITC-Phalloidin) staining and m–r) calcium (Calcein Blue) stained images. Images are displayed from 0 mm (location underneath the electrode) to 12 mm of the gradients. FLAT = flat Si. The arrow underneath the figure shows the direction of the electrical field. The percentage of CB-stained colony area is displayed in the images m-r. Scale bar = 400 μm for a–f) 40× images and 200 μm for g–r) 100× images.

rMSCs (Figure 7g–l). A cell density gradient was observed after osteogenic induction. No obvious CB-positive colonies were found at 0 mm of the gradient after 3 week osteogenesis (Figure 7g,m). However, colonies were found from the 6 mm to the 12 mm of the gradient, as well as at the flat Si, with a gradual increase in frequency and colony size along this direction (Figure 7h–i). The CB-positive cell was normalized to the total cell along the entire gradient to evaluate the osteogenesis of rMSCs. The results show that the fraction of CB-stained cells increased gradually from 14.4 ± 5.2% at 0 mm to 66.4 ± 10.1% at 12 mm of the gradient (Figure 7m–q), while the fraction of CB-stained cells was 29.1 ± 8.4% on the flat Si (Figure 7r). In addition, the fraction of CB-stained cells at the 6 mm of the gradient (34.3 ± 9.9%) was comparable with that on the flat Si.

Although previous studies have demonstrated that the surface nanotopography affected lineage commitment of osteogenic expression,[37,38] few have systematically investigated the influence of porous topography on the osteogenesis of MSCs on a single substrate. Herein, we screened the topography effect on rMSCs using a single n-pSi gradient substrate and demonstrated that the osteogenesis of rMSCs was enhanced by porous topography. Admittedly, cell density or cell-cell interaction could modulate the osteogenesis of MSCs.[39] The non-contact signaling via secreted chemicals (endocrine, autocrine, paracrine etc.)[40] that may stimulate osteogenesis also have to be considered. High local cell density might increase the availability of these secreted biochemicals to the neighbouring cells and result in higher differentiation potential.[41] However, the observed similarity in cell density and morphology for the location 12 mm of the gradient and for flat Si means that osteogenesis of rMSCs can be compared regarding the effect of surface topography. Osteogenesis of rMSCs at the region of 6-12 mm, where the ridge roughness was lower than 10 nm with submicron pores of 20-300 nm, was significantly higher than that at the flat Si. Therefore, we conclude that the optimal porous topography modulates rMSCs attachment, and subsequently enhanced the osteogenesis of rMSCs.

After 6 day culture, rMSCs were adipogenic induced and the effect of porous topography on the adipogenesis of rMSCs was screened up to 2 weeks on the n-pSi gradients (**Figure 8**). Over

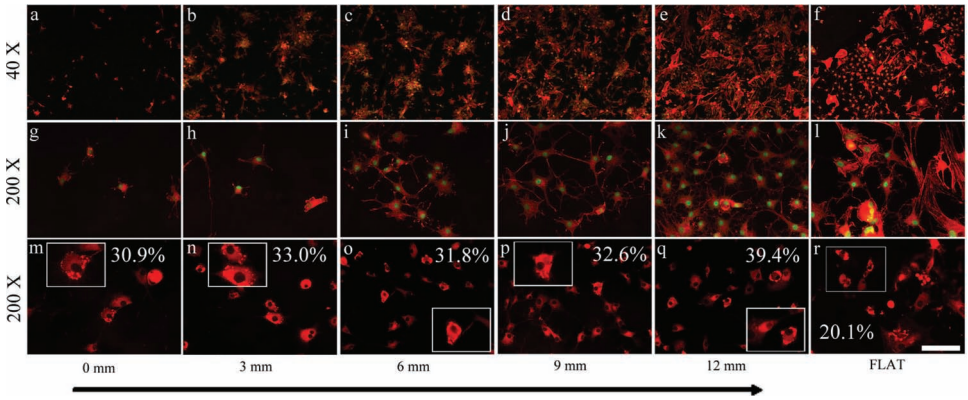

Figure 8. Adipogenesis of rMSCs on the n-type pSi gradients after 2 week induction with a–l) representing merged images of nuclei (PICO Green) and F-actin (TRITC-Phalloidin) staining and m–r) lipid droplet (Nile Red) stained images. Images are displayed from 0 mm (location underneath the electrode) to 12 mm of the gradients. FLAT = flat Si. The arrow underneath the figure shows the direction of the electrical field. The percentage of lipid-laden cell is displayed in the images m-r. Scale bar = 400 μm for a–f) 40× images and 100 μm for g–r) 200× images.

this time, rMSCs became adipocyte-like cells with elongated cell protrusions and secreted lipid droplets stained by Nile Red (NR) were observed around the cells along the entire gradient (Figure 8g–l). A cell density gradient was observed after adipogenic induction. The percentage of lipid droplet-laden cells was quantified along the gradient to evaluate the adipogenesis of rMSCs. The percentage of lipid droplet-laden cells showed no significant difference along the n-pSi gradient from 0 mm (30.9 ± 5.6%) to 12 mm of gradient (39.4 ± 8.6%), but was slightly lower on the flat Si (20.1 ± 6.1%). This result indicates that porous topography also enhanced adipogenesis of rMSCs and that adipogenesis was independent on cell density and surface topography.

Although the role of textured surfaces has been studied widely in the context of osteogenesis of MSCs, few studies have focused on the effect of porous topography on adipogenesis of MSCs. One previous study on the adipogenesis of preadipocyte has demonstrated that polyethylene terephthalate (PET) with nanotextured roughness (Ra = 19.0 ± 2.4 nm) enhanced mouse 3T3-L1 preadipocyte differentiation into lipid-laden fat cells after a 1 week induction period.[42] In addition, another study showed that the adipogenic differentiation of MSCs had no direct relationship to the cell density.[43] The present study using a single n-pSi gradient substrate further demonstrated that adipogenesis of rMSCs was enhanced on porous topography across a wide range of submicron pores and surface roughness values.

3. Conclusions

In the present study, the attachment and differentiations of rMSCs on an n-pSi topography gradient substrate that was stable in cell culture for four weeks were evaluated. Cell attachment was interrelated with the n-pSi topography gradient, especially the ridge roughness, which generated a cell density gradient and ridge roughness gradient with an inverse correlation along the surface. Osteogenesis of rMSCs was found to be enhanced by a porous topography with a ridge roughness lower than 10 nm and abundant submicron pores compared with those higher roughness area as well as flat Si, while adipogenesis of rMSCs was generally enhanced by the porous topography regardless of the feature size. To the best of our knowledge, this is the first report of fabricating n-type pSi gradients for long-term in vitro cell culture studies. This study provides a novel high-throughput format for long-term screening and studying of topography effects on mammalian cell behavior. The results presented in this study are expected to facilitate the development of advanced biomaterials for orthopaedic, tissue engineering and stem cell biology applications.

4. Experimental Section

Materials: Phosphorous-doped n-type silicon wafers with <100> orientation and a resistivity of 0.008–0.02 Ωcm were purchased from Siltronix, France. NCW-1001 surfactant (polyoxyalkylene alkyl ether 30% (w/w) aqueous solution) was purchased from Wako Pure Chemical Industries, Japan. Absolute ethanol and 49% aqueous hydrofluoric acid (HF) solution was purchased from Merck, Australia. Dulbecco's Modified Eagle's Medium low-glucose (DMEM-LG), MEM non-essential amino acid, and Nile Red were purchased from Invitrogen (Carlsbad, USA). All other chemicals were purchased from Sigma-Aldrich (St. Louis, USA) unless specified otherwise.

The culture medium consisted of 90% (v/v) DMEM-LG containing 2 mM L-glutamine, 100 U mL^{-1} penicillin (Invitrogen), 100 g mL^{-1} streptomycin (Invitrogen), 0.25 g mL^{-1} amphotericin (Invitrogen), 0.1 mM MEM non-essential amino acids, and 10% fetal bovine serum (JRH, Australia) with pH 7.4. Phosphate buffered saline (PBS) consisted of NaCl (137 mM), KCl (2.7 mM), Na_2HPO_4 (10 mM), and KH_2PO_4 (1.8 mM) with pH 7.4.

Porous Silicon Gradient Fabrication: Porous silicon (pSi) gradients were prepared from highly phosphorus-doped n-type silicon wafers based on the setup previously described by Khung et al.[17] The n-type silicon was etched in a 25:200:1 (v/v/v) solution of 49% aqueous HF:H_2O:surfactant by placing a Pt electrode perpendicular to the silicon surface at one end of the 12 mm-diameter circular chamber made from PTFE (Figure 1A). A two-step etching procedure of 300 mA cm^{-2} for 1.7 s and then subsequently 45 mA cm^{-2} for 50 s was used. The distance between Pt electrode and wafer surface was 1.5 cm. After etching, the samples were rinsed with ethanol, methanol, acetone and dichloromethane and dried under a stream of N_2. The freshly etched pSi surfaces were thermally oxidized in a tube furnace at 400 °C for 30 min and then at 800 °C for 60 min. Once cooled, the samples were further oxidized with an ozone stream of 100 L h^{-1} for 10 min to generate surface hydroxyl groups. Subsequently the samples were coated with 100 mM aminopropyltriethoxy silane (APTES) in dry toluene for 5 min, rinsed with copious amounts of toluene and dried under a stream of N_2.

Characterization of pSi Gradients: Surface pore size and hydrophilicity along the pSi gradients from the region directly under the Pt electrode (0 mm) to the region furthest from the electrode (12 mm) were examined using scanning electron microscopy (SEM, FEI Helios nanolab, USA), atomic force microscopy (AFM, Nanoscope IV Multimode, Veeco, Santa Barbara, USA) and water contact angle (WCA) measurements, respectively. For SEM experiments, samples were sputter-coated with an approximately 5 nm thick layer of platinum to reduce charging effects and enhance the resolution. The pore diameter and thickness of the porous layer on pSi gradients were determined from the top view and cross section of the porous layer, respectively, using ImageJ software (NIH Image, Bethesda, USA). The solid surface fraction along the pSi gradients was determined using solid area divide to total surface area from the SEM images. AFM experiments were carried out in tapping mode with a scan rate of 0.5 Hz and a scan area of 5 × 5 μm^2. Ridge roughness was determined using a selected area on AFM images of 50 nm × 50 nm on the ridge. Surface wettability along the pSi gradients was determined using sessile drop WCA measurements. Deposited water droplets had a volume of 1 µL and were deposited at five positions along the gradient with an interval of 3 mm. Images of the deposited droplets were captured by a camera and the contact angle on both sides of the water droplets were determined using ImageJ software ($n = 6$).

Rat Mesenchymal Stem Cell Culture: Female Wistar rats (~100 g per animal, Animal Care Unit, Flinders University) were sacrificed by anaesthesia under the guidelines approved by the Flinders University Animal Care and Utilization Committee as described in a previous study[44]. Briefly, bone marrow cells were collected from the femurs and tibias by flushing the bone with culture medium. Cells were filtered through a 100 µm nylon mesh and subjected to a red blood cell lysis solution (0.15 M ammonium chloride, 10 mM potassium bicarbonate, 0.1 mM EDTA) for 5 min. After centrifugation, cells were resuspended in culture medium. After 24 h incubation at 37 °C and 5% CO_2, non-adherent cells were discarded and the adherent cells were grown to 90% confluence in fresh culture medium. The medium was replaced every 3 days until the cells reached confluence. Rat mesenchymal stem cells (rMSCs) were detached by trypsinization and collected by centrifugation at 100 × g for 10 min as passage 1 cells. For this study, passage 2 cells were used exclusively.

rMSCs Attachment and Proliferation on pSi Gradients: Prior to seeding cells, pSi gradients were sterilized using 70% ethanol for 10 min, rinsed with copious amounts of sterile PBS and transferred into a 6-well plate (Iwaki, Japan). For cell attachment tests, a cell density of 20,000 cells cm^{-2} was seeded on the n-pSi gradients for 24 h. In long-term studies, a

cell density of 40,000 cells cm^{-2} was seeded. Cells were cultured for 6 d to examine cell proliferation. After either 24 h or 6 d in culture, cells were fixed using 4% paraformaldehyde and nuclei were stained with DAPI (500 nM). The number of nuclei across the gradients from 0 mm to 12 mm of the gradients was counted both for the 24 h and the 6 d samples ($n = 3$).

For morphology observation, cells were fixed with 4% paraformaldehyde for 30 min. The samples were cut in half symmetrically along the length of the gradient. One half was then incubated with 500 nM Phalloidin-TRITC (for F-actin staining) and 100 nM DAPI (for nuclei staining) overnight. The cytoskeleton of cells on the gradients was imaged using a fluorescence microscope (Nikon Eclipse 50i) and processed using NIS-Elements BR 3.0x software. The other half of the sample was then dehydrated in graded ethanol of 50, 70, 80, 90, 95%, and then twice in absolute ethanol. After drying in the lamina flow hood, the samples were sputtered with platinum and imaged using SEM (FEI Helios Nanolab).

Differentiation of rMSCs on n-pSi Gradients: After 6 d in culture, the culture medium was replaced by either osteogenic or adipogenic medium to induce rMSCs differentiation. Osteogenesis of rMSCs was examined for a further 3 weeks culture in osteogenic medium (culture medium supplements dexamethasone (30 nM), β-glycerophosphate (10 mM), and ascorbic acid (50 μM)). After the 3 week incubation period, calcium deposition within bone nodules-like colonies was detected by Calcein Blue (CB) staining. Samples were stained using a CB solution (30 μM) overnight in the dark. A CB stock solution (3 mM) was prepared in 25 mM KOH. The solution was then diluted 100-fold in culture medium to prepare the working solution. After staining, samples were rinsed with PBS, followed by fixation with 4% paraformaldehyde for 20 min. The percentage of CB-positive colony area was defined by the area of CB-positive colony area divided by the total colony area in each image. The colony area and CB-positive colony area were calculated automatically using ImageJ software.

Adipogenesis of rMSCs was examined for a further 2 weeks culture in adipogenic medium (culture medium supplements dexamethasone (100 nM), indomethacin (6 μM), insulin (5 μg mL^{-1}), and 3-isobutyl-1-methylxanthine (0.5 mM)). After incubation for 2 weeks, intracellular lipid droplets were stained by Nile Red (NR). Samples were rinsed with PBS, followed by fixation with 4% paraformaldehyde for 20 min, and then stained by NR (10 μg mL^{-1} in methanol) overnight in the dark. The percentage of NR-positive cells was defined by the number of cells with lipid droplet divided by the total number of cells in each image.

Samples were also stained with 500 nM Phalloidin-TRITC and 100 nM DAPI overnight. Fluorescence microscopy images across the gradients were captured by an upright microscope (Nikon Eclipse 50i) and processed using NIS-Elements BR 3.0x software.

Statistical Analysis: Statistical analysis was performed using GraphPad Instat 3.0 software (GraphPad Software, USA). The statistical analysis between each group was determined using One Way ANOVA and Student-Newman-Keuls multiple comparison tests. $p < 0.05$ was considered statistically significant.

Supporting Information

Supporting Information is available from the Wiley Online Library or from the author.

Acknowledgements

The authors gratefully acknowledge funding from the Australian Research Council. P.-Y.W. acknowledges support from the National Science Council (Taiwan) by award of a travel scholarship under the Graduate Program for Studying (GPS) in Australia/New Zealand scheme (98-2911-I-002-056). L.C. acknowledges support form the CSIRO Food Futures Flagship.

Received: February 13, 2012
Revised: April 11, 2012
Published online: May 10, 2012

[1] R. Langer, D. A. Tirrell, *Nature* **2004**, *428*, 487.
[2] A. J. Keung, S. Kumar, D. V. Schaffer, *Annu. Rev. Cell Dev. Biol.* **2010**, *26*, 533.
[3] W.-B. Tsai, J.-H. Lin, *Acta Biomater.* **2009**, *5*, 1442.
[4] W. Sun, J. E. Puzas, T. J. Sheu, X. Liu, P. M. Fauchet, *Adv. Mater.* **2007**, *19*, 921.
[5] P.-Y. Wang, J. Yu, J.-H. Lin, W.-B. Tsai, *Acta Biomater.* **2011**, *7*, 3285.
[6] P.-Y. Wang, H. Thissen, W.-B. Tsai, *Biotechnol. Bioeng.* DOI:10.1002/bit.24452.
[7] J. Y. Lim, H. J. Donahue, *Tissue Eng.* **2007**, *13*, 1879.
[8] A. V. Sapelkin, S. C. Bayliss, B. Unal, A. Charalambou, *Biomaterials* **2006**, *27*, 842.
[9] S. P. Low, N. H. Voelcker, L. T. Canham, K. A. Williams, *Biomaterials* **2009**, *30*, 2873.
[10] D. Fan, G. R. Akkaraju, E. F. Couch, L. T. Canham, J. L. Coffer, *Nanoscale* **2011**, *3*, 354.
[11] M. A. Whitehead, D. Fan, P. Mukherjee, G. R. Akkaraju, L. T. Canham, J. L. Coffer, *Tissue Eng. Part A* **2008**, *14*, 195.
[12] A. Jane, R. Dronov, A. Hodges, N. H. Voelcker, *Trends Biotechnol.* **2009**, *27*, 230.
[13] S. P. Low, K. A. Williams, L. T. Canham, N. H. Voelcker, *Biomaterials* **2006**, *27*, 4538.
[14] S. D. Alvarez, A. M. Derfus, M. P. Schwartz, S. N. Bhatia, M. J. Sailor, *Biomaterials* **2009**, *30*, 26.
[15] T. Bocking, K. A. Kilian, K. Gaus, J. J. Gooding, *Adv. Funct. Mater.* **2008**, *18*, 3827.
[16] B. E. Collins, K. P. S. Dancil, G. Abbi, M. J. Sailor, *Adv. Funct. Mater.* **2002**, *12*, 187.
[17] Y. L. Khung, G. Barritt, N. H. Voelcker, *Exp. Cell Res.* **2008**, *314*, 789.
[18] L. R. Clements, P.-Y. Wang, F. Harding, W.-B. Tsai, H. Thissen, N. H. Voelcker, *Phys. Status Solidi A* **2011**, *208*, 1440.
[19] K. A. Kilian, T. Bocking, J. J. Gooding, *Chem. Commun.* **2009**, 630.
[20] A. A. Agrawal, B. J. Nehilla, K. V. Reisig, T. R. Gaborski, D. Z. Fang, C. C. Striemer, P. M. Fauchet, J. L. McGrath, *Biomaterials* **2010**, *31*, 5408.
[21] L. T. Canham, *Adv. Mater.* **1995**, *7*, 1033.
[22] D. M. Reffitt, R. Jugdaohsingh, R. P. H. Thompson, J. J. Powell, *J. Inorg. Biochem.* **1999**, *76*, 141.
[23] C. M. Thompson, M. Nieuwoudt, A. M. Ruminski, M. J. Sailor, G. M. Miskelly, *Langmuir* **2010**, *26*, 7598.
[24] M. F. Pittenger, A. M. Mackay, S. C. Beck, R. K. Jaiswal, R. Douglas, J. D. Mosca, M. A. Moorman, D. W. Simonetti, S. Craig, D. R. Marshak, *Science* **1999**, *284*, 143.
[25] O. Z. Fisher, A. Khademhosseini, R. Langer, N. A. Peppas, *Acc. Chem. Res.* **2010**, *43*, 419.
[26] R. B. Vasani, S. J. McInnes, M. A. Cole, A. M. Jani, A. V. Ellis, N. H. Voelcker, *Langmuir* **2011**, *27*, 7843.
[27] J. M. Curran, R. Chen, J. A. Hunt, *Biomaterials* **2005**, *26*, 7057.
[28] R. N. Wenzel, *Ind. Eng. Chem.* **1936**, *38*, 988.
[29] A. B. D. Cassie, S. Baxter, *Trans. Faraday Soc.* **1944**, *40*, 546.
[30] P.-Y. Wang, H.-T. Yu, W.-B. Tsai, *Biotechnol. Bioeng.* **2010**, *106*, 285.
[31] F. Luthen, R. Lange, P. Becker, J. Rychly, U. Beck, J. G. Nebe, *Biomaterials* **2005**, *26*, 2423.
[32] X. Zhu, J. Chen, L. Scheideler, T. Altebaeumer, J. Geis-Gerstorfer, D. Kern, *Cells Tissues Organs* **2004**, *178*, 13.
[33] N. R. Washburn, K. M. Yamada, C. G. Simon, Jr., S. B. Kennedy, E. J. Amis, *Biomaterials* **2004**, *25*, 1215.
[34] A. R. Costa-Pinto, A. J. Salgado, V. M. Correlo, P. Sol, M. Bhattacharya, P. Charbord, R. L. Reis, N. M. Neves, *Tissue Eng. Part A* **2008**, *14*, 1049.
[35] B. Neuhuber, S. A. Swanger, L. Howard, A. Mackay, I. Fischer, *Exp. Hematol.* **2008**, *36*, 1176.
[36] K. S. Brammer, C. Choi, C. J. Frandsen, S. Oh, S. Jin, *Acta Biomater.* **2011**, *7*, 683.

[37] M. J. P. Biggs, R. G. Richards, N. Gadegaard, R. J. McMurray, S. Affrossman, C. D. W. Wilkinson, R. O. C. Oreffo, M. J. Dalby, *J. Biomed. Mater. Res. Part A* **2009**, *91A*, 195.
[38] I. Wall, N. Donos, K. Carlqvist, F. Jones, P. Brett, *Bone* **2009**, *45*, 17.
[39] K. A. Purpura, J. E. Aubin, P. W. Zandstra, *Stem Cells* **2004**, *22*, 39.
[40] F. Fagotto, B. M. Gumbiner, *Dev. Biol.* **1996**, *180*, 445.
[41] J. Tang, R. Peng, J. Ding, *Biomaterials* **2010**, *31*, 2470.
[42] Y. Xie, T. Sproule, Y. Li, H. Powell, J. J. Lannutti, D. A. Kniss, *J. Biomed. Mater. Res.* **2002**, *61*, 234.
[43] H. Lu, L. Guo, M. J. Wozniak, N. Kawazoe, T. Tateishi, X. Zhang, G. Chen, *Biochem. Biophys. Res. Commun.* **2009**, *381*, 322.
[44] P. Y. Wang, W. B. Tsai, N. H. Voelcker, *Acta Biomater.* **2012**, *8*, 519.